The Jovian Ionospheric Alfvén Resonator and Auroral Particle Acceleration

R. L. Lysak[1], Y. Song[1], S. Elliott[1,2], W. Kurth[2], A. H. Sulaiman[2], and D. Gershman[3]

[1]Minnesota Institute for Astrophysics, School of Physics and Astronomy, University of Minnesota, Minneapolis, MN, USA.

[2]Department of Physics and Astronomy, University of Iowa, Iowa City, IA, USA

[3]Goddard Space Flight Center, Greenbelt, MD, USA

Key Points:

- Broadband acceleration of auroral particles, which is more prevalent at Jupiter than at Earth, can be achieved by Alfvén waves propagating in the ionospheric Alfvén resonator, a region formed by the rapid increase in the Alfvén speed above the ionosphere.
- Modeling of the Jovian ionospheric Alfvén resonator indicate that electrons could be accelerated to the 10-100 keV range for observed levels of Alfvén wave activity.
- In addition to the ionospheric resonator, there is also an Alfvén resonator in the high-Alfvén speed velocity region between the ionosphere and the dense plasma sheet.

Abstract

The ionospheric Alfvén resonator (IAR) is a structure formed by the rapid decrease in the plasma density above a planetary ionosphere. This results in a corresponding increase in the Alfvén speed that can provide partial reflection of Alfvén waves. At Earth, the IAR on auroral field lines is associated with the broadband acceleration of auroral particles, sometimes termed the Alfvenic aurora. This arises since phase mixing in the IAR reduces the perpendicular wavelength of the Alfvén waves, which enhances the parallel electric field due to electron inertia. This parallel electric field fluctuates at frequencies of 0.1-20.0 Hz, comparable to the electron transit time through the region, leading to the broadband acceleration. The prevalence of such broadband acceleration at Jupiter suggests that a similar process can occur in the Jovian IAR. A numerical model of Alfvén wave propagation in the Jovian IAR has been developed to investigate these interactions. This model describes the evolution of the electric and magnetic fields in the low-altitude region close to Jupiter that is sampled during Juno's perijove passes. In particular, the model relates measurement of magnetic fields below the ion cyclotron frequency from the MAG and Waves instruments on Juno and electric fields from Waves to the associated parallel electric fields that can accelerate auroral particles.

Plain Language Summary:

Just like at Earth, the polar regions of the planet Jupiter are circled by a luminous aurora (northern and southern lights) that can be seen from telescopes like the Hubble Space Telescope near Earth. The aurora on both planets is produced by electrons impacting the upper atmosphere, causing the atoms and molecules in this region to emit light. At Earth, these electrons are mainly produced by large voltages that cause all the electrons to be accelerated to nearly the same energy. However, recent observations from the Juno satellite at Jupiter shows that these electrons are mainly accelerated over a broad range of energies. This suggests that the voltages accelerating these electrons are fluctuating rapidly in time. Such fluctuations can be caused by the strong increase in the effective wave speed due to a rapid decrease in the number of electrons as the altitude is increased. We have developed a computer model to help understand these interactions.

Index terms: 2752 MHD Waves and Instabilities, 2756 Planetary Magnetospheres, 2704 Auroral Phenomena, 2753 Numerical Modeling, 2736 Magnetosphere/Ionosphere interactions

Key Words: Jupiter, kinetic Alfvén waves, aurora, magnetosphere-ionosphere coupling.

1. Introduction

The aurora at Jupiter is presently being investigated by the NASA Juno satellite, which went into a polar orbit around Jupiter on July 4, 2016 (e.g., Bagenal et al., 2017). Observations of auroral particles at Earth show that the most common form of auroral acceleration is a monoenergetic beam thought to be caused by a parallel potential drop (e.g., Gurnett & Frank, 1973; Mozer et al., 1980). However, in other cases, the aurora is associated with electrons having a broadband distribution in energy (e.g., Chaston et al., 2002; Semeter & Blixt, 2006). However, the measurements from Juno indicate that the aurora at Jupiter is commonly associated with broadband electrons, in contrast to the situation at Earth (e.g., Allegrini et al., 2020; Mauk et al., 2017). Monoenergetic beams of electrons are also present at Jupiter, but are less common.

The electrons that produce the discrete aurora are generally thought to be associated with the acceleration of these electrons by electric fields parallel to the background magnetic field. The monoenergetic electrons are produced by a quasi-static parallel electric field that accelerates all the electrons to the same energy (e.g., Karlsson, 2012). A broadband acceleration of these electrons would require that the parallel electric field would vary over the time it takes for the electrons to pass through the acceleration region. One possibility would be through the excitation of whistler-mode waves (Elliott et al., 2018); however, the excitation of these waves requires a pre-existing beam of electrons. The other possibility, and one that is more widely accepted in the case of Earth, is the production of kinetic Alfvén waves in the so-called ionospheric Alfvén resonator that carry a parallel electric field that fluctuates on a time scale of a few seconds, sufficient to accelerate these particles (e.g., Lysak, 1991, 1993; Watt & Rankin, 2009). It is the purpose of this paper to examine the effects of Alfvén waves in the ionospheric Alfvén resonator (IAR) in the context of the Jovian magnetosphere.

The ionospheric Alfvén resonator, first recognized in spectral signals associated with ionospheric heating experiments (Polyakov & Rapaport, 1981), is a structure formed by the rapid decrease of the mass density of the plasma with altitude above the ionosphere. This structure leads to a rapid increase in the Alfvén speed, which gives the propagation velocity of Alfvén waves, waves analogous to waves on a string that propagate along magnetic field lines in a plasma. The Alfvén speed is given by $V_A = B/\sqrt{\mu_0 \rho}$ in cases where this speed is much less than the speed of light. However, at Jupiter, and even to some extent at Earth, this speed can approach the speed of light, in which case it is modified, with the modified speed denoted by c_A:

$$c_A = \frac{V_A}{\sqrt{1 + V_A^2 / c^2}} \tag{1}$$

Over the auroral zone at Jupiter, the Alfvén speed will approach the speed of light at altitudes less than 1 Jovian radius (1 R_J = 71492 km) over the surface of Jupiter, which is taken to be at the 1 bar level (e.g., Weiss, 2004). The rapid increase in the Alfvén speed causes the partial reflection of Alfvén waves so that they can be quasi-trapped in the resonator. At both Earth and Jupiter, the resonant frequencies of the IAR are in the 0.1-20.0 Hz range (Lysak, 1991; Su et al., 2006). At small wavelengths perpendicular to the field, the effect of finite electron inertia becomes significant and leads to a parallel electric field that will fluctuate at the IAR resonant frequency. As a reference point, an electron traveling at one planetary radius per second has an energy of about 100 eV at Earth and 15 keV at Jupiter.

This paper will consider a numerical model of the IAR at Jupiter based on measurements from Juno. The Waves instrument on Juno (Kurth et al., 2017) can make estimates of the electron density by observing resonances and cutoffs in the wave emissions (Elliott et al., 2021) that can serve as an input to the model. In some cases these measurements can be confirmed by direct particle measurements from the Jovian Auroral Distributions Experiment (JADE; Allegrini et al., 2020; McComas et al., 2013). In addition, the MAG magnetometer experiment (Connerney et al., 2017) has made direct measurements of the magnetic fields of the Alfvén waves near perijove (Gershmann et al., 2019). Alfvén waves at frequencies above 50 Hz have also been observed by Waves (Sulaiman et al., 2020). These measurements can be used to constrain the amplitudes of the Alfvén waves excited in our model.

The remainder of this paper will be organized as follows. First, the theory of the ionospheric Alfvén resonator will be considered in general terms. Then we will discuss the numerical model and its application to the Jovian magnetosphere. This will be followed by a discussion of the formation of parallel electric fields and comparison with the potentials needed to accelerate the Jovian electrons. We will conclude with a discussion of the results and plans for future work.

2. Theory of the Ionospheric Alfvén Resonator

The ionospheric Alfvén resonator (IAR) is formed by the rapid decrease in the plasma density with altitude above the ionospheric peak, leading to a rapid increase in the Alfvén speed. The IAR has been frequently invoked in the Earth's auroral zone and associated with the acceleration of auroral electrons (e.g., Cohen et al., 2013; Hebden et al., 2005; Hirano et al., 2005; Lynch et al., 2015; Lysak, 1991, 1993; Lysak & Song, 2008; Lysak et al., 2013; Miles et al., 2018; Pakhotin et al., 2018; Polyakov & Rapaport, 1981; Sydorenko et al., 2008; Trakhtengertz & Feldstein, 1984; Woodroffe & Lysak, 2012). It has also been suggested to have an effect on auroral radio emissions at Jupiter (Ergun et al., 2006; Su et al., 2006). Perhaps the best measurements of ionospheric densities in the Jovian ionosphere have been made from radio occultation measurements from Galileo (Hinson et al., 1997) and Voyager 2 (Hinson et al., 1998), which saw peak densities of the order of 10^5 cm^{-3} while more recent radio occultation measurements from Juno suggest densities could be as high as 10^9 cm^{-3} (Hodges et al., 2020). At higher altitudes, electron densities determined from wave cutoffs and resonances indicate densities below 2 R_J of less than 100 cm^{-3} and sometimes as low as 1 cm^{-3} (Elliott et al., 2021). Thus, the conditions for the existence of an ionospheric Alfvén resonator are clearly present on auroral field lines at Jupiter.

A simple theoretical model of the IAR was presented by Lysak (1991), based on an Alfvén speed profile first introduced by Trakhtengertz and Feldstein (1984):

$$V_A^2(z) = \frac{V_{AI}^2}{\varepsilon^2 + e^{-z/h}} \tag{2}$$

Here V_{AI} is the Alfvén speed in the ionosphere, $\varepsilon = V_{AI}/V_{AM}$ where V_{AM} is the magnetospheric Alfvén speed and h is the density scale height. This profile is plotted in Figure 1. Inserting this profile in the wave equation for shear Alfvén waves at a frequency ω gives

$$\frac{d^2\Phi}{dz^2} + \frac{\omega^2}{V_{AI}^2}\left(\varepsilon^2 + e^{-z/h}\right)\Phi = 0 \tag{3}$$

Solutions to this equation can be found by using the substitution $x = x_0 e^{-z/2h}$, where $x_0 = 2h\omega/V_A$. This transforms equation (3) into a form of Bessel's equation with the general solutions:

$$\Phi = A_{inc} J_{ix_0\varepsilon}\left(x\right) + A_{ref} J_{-ix_0\varepsilon}\left(x\right) \tag{4}$$

Here A_{inc} and A_{ref} are the amplitudes of the incident and reflected Alfvén waves, respectively. In the limit of $\alpha = \mu_0 V_{AI} \Sigma_P >> 1$, which is often the case, the eigenfrequencies of these modes (i.e., the frequencies that admit a pure incident or reflected wave) are given by $\omega_n = \xi_n V_{AI}/2h$, where ξ_n is the nth zero of the zeroth order Bessel function, 2.4, 5.5, 8.6,… For the profile of Figure 1, the lowest eigenfrequency is 0.8 Hz.

Figure 2 illustrates the structure of these modes as a function of frequency and altitude. This figure plots the logarithm of the total wave field normalized to the amplitude of the incident wave as a function of frequency and the distance along the field line. The enhancement of the wave amplitude at lower altitudes at $2h\omega/V_A$ = 2.4, 5.5, 8.6 can be clearly seen in the Figure. For comparison with the model to be discussed in the next section, this plot assumes α = 18.5 and ε = 0.05. The typical crossing of the auroral zone during the early perijoves of the Juno mission at an altitude of 0.7 R_J corresponds to z/h = 18.5 on this plot.

3. Numerical model for the IAR at Jupiter

Next we would like to apply the theory of the IAR to conditions in the main auroral region of Jupiter. We have developed a numerical model similar to the one used in Lysak and Song (2020) based on the Connerney et al. (2020) current sheet model and the Bagenal and Delamere (2011) plasma model. We will concentrate on the region around a co-latitude of 17°, which for this model corresponds to M = 23 (here M refers to the equatorial crossing distance of the field line in units of Jovian radii). As in Lysak and Song (2020), we use magnetic coordinates where the flux function ν (equal to the vector potential times the distance from the magnetic axis) labels each field line, and the parallel coordinate μ is taken to be the magnetic scalar potential. Here the ν coordinate is directed southward (at the ionosphere) and the μ coordinate increases upward. The usual eastward azimuthal coordinate φ completes the set. Explicit forms of these coordinates are described in Lysak and Song (2020). However, in contrast to the previous model, we will focus on the lower parts of the field line to emphasize the dynamics in the IAR and model only one hemisphere, which will be the northern hemisphere in the results presented here. Figure 3 shows the simulation volume, with representative field lines and lines at constant scalar potential indicated.

Figure 4 shows a typical profile of the Alfvén speed (solid line) and density (dashed line) profiles. It can be seen that this profile closely follows equation (2) until it reaches about 4 R_J where it begins to decrease because of the decrease in the magnetic field. The Alfvén speed is plotted in Figure 5 overlaid on the grid shown in Figure 3. The inset in this figure shows the region of the ionospheric Alfvén resonator. These plots are for an ionospheric density of 2×10^5 cm^{-3} and a scale height of 5000 km.

The simulated equations are Maxwell's equations with a dielectric constant representing the Alfvén wave, supplemented by the cold electron equation of motion along the field line, written in terms of the field-aligned current. We consider only the toroidal Alfvén wave and assume there is no azimuthal variation, so that the wave fields are E_ν, B_φ, E_μ and J_μ. Then the model equations for an ideal MHD Alfvén wave become

$$\frac{\partial E_\nu}{\partial t} = -\frac{1}{\varepsilon_\perp \mu_0}\frac{1}{h_\varphi h_\mu}\frac{\partial\left(h_\varphi B_\varphi\right)}{\partial \mu} \qquad \frac{\partial B_\varphi}{\partial t} = -\frac{1}{h_\nu h_\mu}\left[\frac{\partial\left(h_\nu E_\nu\right)}{\partial \mu} - \frac{\partial\left(h_\mu E_\mu\right)}{\partial \nu}\right] \tag{5}$$

Here $\varepsilon_\perp = \varepsilon_0\,(1+c^2/V_A^2)$, and the scale factors are $h_\varphi = r\sin\theta$, $h_\mu = R_J B_{eq}/B$ where B_{eq} is the magnetic field strength at 1 R_J on the magnetic equator, and $h_\nu = R_J h_\mu / h_\varphi$.

The ideal MHD approximation is violated when the perpendicular wavelength becomes comparable to the electron inertial length, $\lambda_e = \sqrt{m_e / \mu_0 n e^2}$, or the ion acoustic gyroradius, $\rho_s = \sqrt{T_e m_i} / eB$, which despite its common name, depends on the electron pressure, not the gyromotion of any ion (e.g., Goertz & Boswell, 1979; Lysak, 1991). The electron inertial length is the larger of the two scales when the electron thermal speed is less than the Alfvén speed; therefore, the electron inertial length is the most relevant on Jovian field lines in the region less than 30 R_J on field lines threading the main auroral emission (Saur et al., 2018). In this situation, equation (5) is supplemented by Ampere's Law, including the displacement current, and the cold electron equation of motion:

$$\varepsilon_{\parallel}\frac{\partial E_{\mu}}{\partial t} = \frac{1}{\mu_0}\frac{1}{h_{\nu}h_{\varphi}}\frac{\partial (h_{\varphi}B_{\varphi})}{\partial \nu} - J_{\mu} \qquad \frac{\partial J_{\mu}}{\partial t} = \frac{ne^2}{m_e}E_{\mu} \tag{6}$$

The parallel permittivity $\varepsilon_{\parallel}$ is increased from ε_0 to improve the stability of the numerical scheme (Lysak and Song, 2001).

The numerical model can be driven either from the magnetospheric side or the ionospheric side. At the ionosphere, we adopt a simplified current sheet model including only Pedersen currents, since Hall currents tend to be much smaller in the Jovian ionosphere (e.g., Millward et al., 2002). In that case, Ohm's Law integrated over the current sheet can be written as

$$B_{\varphi} = \mu_0 \Sigma_P \left(E_{\nu} \pm V_n B_0 \right) \tag{7}$$

where Σ_P is the ionospheric conductance, B_0 is the background magnetic field and V_n is the azimuthal velocity of the neutral atmosphere in the corotating frame. The top sign is appropriate for the northern hemisphere while the bottom sign is for the south, due to the way we defined the coordinate system. (All the runs shown here are in the northern hemisphere.) The neutral velocity term represents a source for the Alfvén waves, which we take to be fluctuations or turbulence in the neutral atmosphere. It should also be noted that although the code is three-dimensional, for the runs presented in this work the perturbations have been assumed to be uniform in the azimuthal direction, so that the magnetic local time (MLT) label on the plots is not relevant.

We can use this numerical model to examine the theory of the IAR at Jupiter. First, we will consider the ideal MHD case, in which case only the equations (5) are simulated. For this run, the density at the ionosphere was set to 2×10^{6} cm^{-3} and it then decreases exponentially with a scale height of 2500 km (0.035 R_J). However, because of the decrease in the magnetic field strength, which is not included in the analytic model described above, the effective scale height for the Alfvén speed is about 3500 km. From the theory of the IAR, this would lead to a fundamental resonance frequency of 0.8 Hz with the next harmonic at 1.8 Hz.

The simulation is driven by a pulse in the neutral velocity lasting 0.25 seconds with an amplitude of 1.25 km/s, leading to a 1 V/m electric field in the 8 G field at this latitude, simulating a flow burst in the neutral atmosphere (e.g., Yates et al., 2014, 2020). Figure 6 shows the time history of the electric and magnetic fields as measured at 1.7 R_J, a typical distance for the auroral crossings in the early Juno perijoves. It can be seen that the fields are not simply an image of the input pulse; rather there is structure in the pulses and they repeat due to reflections due to the gradient in the Alfvén speed. Figure 7 shows the Fourier transform of the electric field, indicating the peaks are at 0.8 and 1.8 Hz, consistent with the theory.

Another way of considering the importance of the IAR is the response to a monochromatic driving. Figure 8 shows the magnetic field observed at 1.7 R_J due to a driving at 0.8 Hz (Figure 8a) and 0.4 Hz (Figure 8b) with the same amplitude as in the previous figures. It can be seen that the resonant case (0.8 Hz) reaches and amplitude of about 10 nT while the off-resonant (0.4 Hz) case only yields about 2 nT. This illustrates the trapping and reflection of waves that are resonant with the IAR cavity.

4. Development of Parallel Electric Fields

As discussed above, the Alfvén wave develops a parallel electric field when the perpendicular wavelength becomes comparable to the electron inertial length. The electron inertial effect can be implemented by including the two equations of equation (6). For a plane wave in a uniform plasma, the parallel electric field due to electron inertia can be written as (e.g., Stasiewicz et al., 2000):

$$E_{\|} = \frac{k_{\|} k_{\perp} \lambda_e^2}{1 + k_{\perp}^2 \lambda_e^2} E_{\perp} \tag{8}$$

To model the development of parallel electric fields in the IAR, we have done simulations using the full set of equations (5) and (6). We use the model shown in Figures 4 and 5, with an ionospheric density of 2×10^5 cm^{-3} and a scale height of 5000 km. This profile gives a density at 1.7 R_J of about 10 cm^{-3}, consistent with the density measured at times when Juno crossed the main auroral emissions (Elliott et al., 2021). The run is driven by an oscillation at 1.0 Hz in the ionospheric electric field, which corresponds to the IAR resonance for this density profile. Figure 9 shows the magnetic perturbation at 1.74 R_J for this run. It can be seen that the magnetic field oscillates with a peak amplitude of about 12 nT, a value somewhat lower than Juno observations with a mean value of 20 nT during PJ1 (Gershman et al., 2019). Figure 10 gives the maximum integrated electric field along a model field line during this run. To make this plot, the parallel electric field is integrated along each field line, and the maximum value on any field line is plotted.

This field increases in a stepwise fashion every 15-20 seconds, reaching values of almost 30 kV by the end of the run. This suggests that significant particle acceleration could be achieved in this wave. It should be emphasized that the parallel electric field here is not a potential field, and so this integrated parallel electric field is not a true potential drop. Nevertheless it does give an indication of the energies that could be achieved by a particle traversing this region.

Figures 9 and 10 raise the question of why the potential drop increases while the magnetic perturbation doesn't grow appreciably. This is due to the reflections of the Alfvén wave at the boundary of the plasma sheet. The Alfvén speed profile for this run was shown in Figures 4 and 5. The Alfvén speed shows a sharp gradient between 9 and 10 R_J where the density starts to increase. A calculation of the Alfvén travel time from the ionosphere indicates that it takes an Alfvén wave about 6-10 seconds to reach this point from the ionosphere. This causes a reflection that reinforces the wave field with a 12-20 second period, indicating the presence of a larger resonant cavity in the high-speed region between the ionosphere and the plasma sheet. Figure 11 shows the field-aligned Poynting flux mapped to the ionosphere at 10, 40, 80, and 120 seconds into this run. Here green, yellow, and red colors indicate an upward Poynting flux, while blue and purple are downward fluxes. An animation of the evolution of the Poynting flux can be found in the supplementary material, Movie S1. A number of features can be seen from this figure and from the movie. First, at 10 seconds, the wave launched from the ionosphere is traveling up the field line and has not yet reached the reflection point. By 40 seconds, the wave has hit the Alfvén speed gradient and has started to reflect, as can be seen in the downward Poynting flux beginning to appear. The Poynting flux doesn't penetrate beyond 10 R_J, indicating a reflection of the Alfvén wave. Secondly, the wave becomes more structured with each successive time frame. This is the result of phase mixing (e.g., Mann et al., 1995; Lysak and Song, 2011), due to the weak plasma density gradients perpendicular to the main field. This occurs since the resonant frequency of this high-Alfvén speed cavity is slightly different on each field line, leading to a structuring of the wave. Because of the decreasing perpendicular scales, the field-aligned current density (not shown) and the parallel electric field shown in Figure 10 increase with each bounce even though the magnetic perturbation remains roughly constant.

As has been known in the case of the Earth's magnetosphere (e.g., Chaston et al., 2006; Persoon et al., 1988; Song and Lysak, 2006), the formation of parallel electric fields is favored by low plasma densities. Our runs indicate that this is also the case at Jupiter. A run similar to the run shown in Figures 9-11 but with the scale height decreased to 4100 km (giving a density of 1 cm^{-3} at 1.7 R_J) is shown in Figure 12. In this case, the magnetic perturbation and the parallel potential rise in a stepwise fashion to values over 20 nT and up to almost 100 kV. These increases are again due to reflections between the ionosphere and the Alfvén speed gradient at large radial distance. Furthermore, another run where the minimum density in the lobes was set to 10 cm^{-3} produced potentials of less than 50 V. This confirms that strong parallel electric fields are favored by low density, as at Earth.

5. Discussion and Conclusions

This work has shown that the structure of the Alfvén speed with altitude on auroral field lines is critical in the evolution of field-aligned currents and parallel electric fields. Alfvén waves are reflected when the gradient scale length in the Alfvén speed is comparable with the wavelength of the wave, so that the WKB approximation is violated. This leads to the formation of resonant cavities in which Alfvén waves can be trapped. It should be noted that these are leaky cavities since the shear Alfvén wave equation (3) does not have a classical turning point, so that wave energy can leak out of the cavity. Nevertheless, the approximate trapping of Alfvén waves in these gradients can lead to an enhancement of the wave amplitude, which in turn leads to enhanced parallel electric fields that can accelerate auroral particles.

At both Earth (e.g., Cummings et al., 1969; Mann et al., 1995; Singer et al., 1981) and Jupiter (Lysak & Song, 2020; Manners et al., 2018; Manners & Masters, 2019), reflections from the conjugate ionospheres can give rise to field line resonances, with periods of a few minutes at Earth and tens of minutes at Jupiter. In addition, the sharp gradients in the Alfvén speed above the ionosphere lead to the formation of an ionospheric Alfvén resonator as described here with periods of seconds. However, the presence of the dense plasma torus due to Io and the resulting plasma disk of high-density plasma at Jupiter can give rise to other resonant cavities. In this work, we have seen the presence of the high Alfvén speed region between the ionosphere and plasma disk can constitute another resonator with periods of tens of seconds. This resonator is unique to Jupiter, and no analog of this exists at Earth. It is worth noting that the reflection point at this gradient is itself a function of the wave frequency since lower frequencies have longer wavelengths. A run like the one in Figures 9-11 except with a lower driving frequency of 0.1 Hz did not reflect before passing out of the simulation volume. Although we have not considered it here, it is also likely that similar resonant cavities can exist in the plasma torus itself (Manners and Masters, 2020).

For these Alfvén waves to give rise to parallel electric fields, two conditions must be met. First, the plasma density must be low. This not only increases the electron inertial length, but also limits the ability of the plasma to carry strong field-aligned currents. In kinetic steady-state models of currents and parallel electric fields, low densities can lead to a "current choke" condition where the current required to balance the curl of **B** becomes greater than a critical current that is the order of $j_{cirt} \sim nev_{th}$, where v_{th} is the electron thermal speed (Ray et al., 2009). When this condition is violated, the displacement current term in the parallel Ampere's Law (i.e., the first term on the right-hand side of the first equation of (6)) becomes important and leads to parallel electric fields (Song & Lysak, 2006). However, we have not included this choke condition in the results presented here. This condition will be included in future work.

The second required condition is that the perpendicular wavelength of the Alfvén waves must become comparable to the electron inertial length or ion acoustic gyroradius. This can be accomplished in a number of ways. First, plasma turbulence can lead to a cascade of energy from large scales to small scales, a process that has been invoked in both Earth (e.g., Chaston et al., 2008) and at Jupiter (Saur et al., 2003, 2018). A second possibility is that shown here, that phase mixing due to perpendicular gradients in the Alfvén speed can lead to smaller wavelengths. This process occurs because the resonant period in the Alfvén resonant cavities is slightly different on adjacent field lines, so that these waves get out of phase with each other. This is demonstrated in Figure 11 showing how the waves trapped in the high-speed resonator develop perpendicular structure. A third possibility is ionospheric feedback. The precipitation of electrons into the ionosphere leads to a localized ionization enhancement, and additional currents will flow at those conductance gradients (e.g., Lysak, 1991; Miura & Sato, 1980). This process will be considered in future work.

Another issue is how these low-density cavities can develop. Measurements from Juno indicate that electron densities below about 2 R_J are around 100 cm^{-3} (Elliott et al., 2021). As we have seen, these densities are too high for significant parallel electric fields to develop. This would suggest that the density cavities form as a result of the magnetosphere-ionosphere interaction. Juno observations indicate that there is a strong proton upflow on auroral field lines (Szalay et al., 2021) as well as on the Io flux tube (Szalay et al., 2018). These upflowing ions may leave behind a density depletion at lower altitudes. One possibility is that these upflowing ions are accelerated by the ponderomotive force of the Alfvén waves (e.g, Rankin et al., 1995; Sydorenko et al., 2008). Another possibility is that they are accelerated by the parallel electric fields themselves, leading to a different type of positive feedback, in which the density cavity is produced by the parallel electric fields, and in turn the parallel electric fields are enhanced by the low plasma densities.

Although the present work has focused on the main auroral emission region, Alfvén waves have long been associated with the coupling of the moon Io with the ionosphere of Jupiter (e.g., Acuña et al., 1981; Bagenal, 1983; Belcher et al., 1981; Chust et al., 2005; Crary, 1997; Goertz, 1980; Gurnett & Goertz, 1981; Hinton et al., 2019; Neubauer, 1980). This process will be the focus of future work; however, it is quite likely that similar magnetosphere-ionosphere coupling processes should be associated with this interaction. It is also likely that the high-speed resonator described here is present on the Io flux tube and may be responsible for the structure observed in the footprint tail of Io and other moons (Moirano et al., 2021; Mura et al., 2018).

In summary, we have presented the theory and modeling of the ionospheric Alfvén resonator as well as the resonator formed by the high-Alfvén-speed region between the ionosphere and the plasma sheet. These resonant structures can lead to large-amplitude Alfvén waves that can lead to structuring of the field-aligned currents due to phase mixing. In low-density regions of the magnetosphere, parallel electric fields can develop due to the effect of electron inertia that can lead to potentials up to 100 kV on auroral field lines. While the overall evolution of the auroral acceleration at Jupiter is a complicated problem, this work has shown that the dynamics of Alfvén waves propagation in the inhomogeneous plasma at Jupiter is a major ingredient in understanding auroral acceleration at Jupiter.

Acknowledgments and Data Availability.

We would like to thank Fran Bagenal for useful comments on this work. Work at the University of Minnesota is supported by NASA grant 80NSSC20K1269 and grant AGS-1840891 from the National Science Foundation. We also acknowledge supercomputer support from the Minnesota Supercomputer Institute. The research conducted at the University of Iowa was supported by NASA through contract 699041X with the Southwest Research Institute. Source code for the

numerical simulations and data files associated with the results presented in this paper are available at the Data Repository for the University of Minnesota (DRUM).

References

Acuña, M. H., Neubauer, F. M., & Ness, N. F. (1981). Standing Alfven wave current system at Io - Voyager 1 observations. *Journal of Geophysical Research, 86*(A10), 8513–8521. http://doi.org/10.1029/JA086iA10p08513

Allegrini, F., Mauk, B., Clark, G., Gladstone, G. R., Hue, V., Kurth, W. S., et al. (2020). Energy flux and characteristic energy of electrons over Jupiter's main auroral emission. *Journal of Geophysical Research: Space Physics, 125,* e2019JA027693. https://doi.org/10.1029/2019JA027693

Bagenal, F. (1983). Alfven wave propagation in the Io plasma torus. *Journal of Geophysical Research, 88*(A4), 3013–3025. https://doi.org/10.1029/JA088iA04p03013

Bagenal F., & P. A. Delamere (2011), Flow of mass and energy in the magnetospheres of Jupiter and Saturn, *J. Geophys. Res., 116,* A05209, doi:10.1029/2010JA016294.

Bagenal, F., Adriani, A., Allegrini, F., Bolton, S. J., Bonfond, B., Bunce, E., et al. (2017), Magnetospheric Science Objectives of the *Juno* mission, *Space Sci. Rev., 213, 219-287,* doi: 10.1007/s11214-014-0036-8.

Belcher, J. W., Goertz, C. K., Sullivan, J. D., & Acuna, M. H. (1981). Plasma observations of the Alfvén wave generated by Io. *Journal of Geophysical Research, 30,* 8508–8512. https://doi.org/10.1029/JA086iA10p08508

Chaston, C. C., Bonnell, J. W., Carlson, C. W., Berthomier, M., Peticolas, L. M. Roth, I. et al. (2002). Electron acceleration in the ionospheric Alfven resonator, *J. Geophys. Res., 107*(A11), 1413, doi:10.1029/2002JA009272,.

Chaston, C. C., V. Genot, J. W. Bonnell, C. W. Carlson, J. P. McFadden, R. E. Ergun, et al. (2006), Ionospheric erosion by Alfvén waves, *J. Geophys. Res., 111,* A03206, doi:10.1029/2005JA011367.

Chaston, C. C., Salem, C., Bonnell, J. W., Carlson, C. W., Ergun, R. E., Strangeway, R. J. & McFadden, J. P. (2008), The turbulent Alfvénic aurora, *Phys. Rev. Lett., 100,* 175003.

Chust, T., Roux, A., Kurth, W. S., Gurnett, D. A., Kivelson, M. G., & Khurana, K. K. (2005). Are Io's Alfven wings filamented? Galileo observations. Planetary and Space Science, 53(4), 395–412. https://doi.org/10.1016/j.pss.2004.09.021

Cohen, I. J., Lessard, J. R., Kaeppler, S. R., Bounds, S. R., Kletzing, C. A., Streltsov, A. S. et al. (2013), Auroral Current and Electrodynamics Structure (ACES) observations of ionospheric feedback in the Alfvén resonator and model responses, *J. Geophys. Res. Space Physics, 118,* doi:10.1002/jgra.50348.

Connerney, J. E. P., Benn, M., Bjarno, J. B., Denver, T., Espley, J., Jorgensen, J. L., et al. (2071). The Juno magnetic field investigation, *Space Science Reviews, 213,* 39-138. doi: 10.1007/s11214-017-0334-z

Connerney, J. E. P., Timmins, S., Herceg, M., & Joergensen, J. L. (2020). A Jovian magnetodisc model for the Juno era. *Journal of Geophysical Research: Space Physics, 125,* e2020JA028138. https://doi.org/10.1029/2020JA028138

Crary, F. J. (1997), On the generation of an electron beam by Io, *J. Geophys. Res. Space Physics, 102,* 37.

Cummings, W. D., O'Sullivan, R. J., & Coleman, P. J. (1969), Standing Alfvén waves in the magnetosphere, *J. Geophys. Res., 74,* 778.

Elliott, S. S., Gurnett, D. A., Kurth, W. S., Mauk, B. H., Ebert, R. W., Clark, G., et al. (2018). The acceleration of electrons to high energies over the Jovian polar cap via whistler mode wave-particle interactions. *Journal of Geophysical Research: Space Physics, 123,* 7523–7533. https://doi.org/10.1029/2018JA025797

Elliott, S. S., Sulaiman, A. H., Kurth, W. S., Faden, J., Allegrini, F., Valek, P. et al. (2021), in press, *Journal of Geophysical Research: Space Physics.*

Ergun, R. E., Su, Y.-J., Andersson, L., Bagenal, F., Delamere, P. A., Lysak, R. L., and Strangeway, R. J. (2006). S bursts and the Jupiter ionospheric Alfvén resonator, *J. Geophys. Res., 111,* A06212, doi: 10.1029/2005JA011253

Gershman, D. J., Connerney, J. E. P., Kotsiaros, S., DiBraccio, G. A., Martos, Y. M., F.-Viñas, A., et al. (2019). Alfvénic fluctuations associated with Jupiter's auroral emissions. *Geophysical Research Letters, 46.* https://doi.org/10.1029/2019GL082951

Goertz, C. (1980). Io's interaction with the plasma torus, *J. Geophys. Res., 85,* 2949-2956.

Goertz, C. K., & Boswell, R. W. (1979) Magnetosphere-ionosphere coupling, *J. Geophys. Res., 84,* 7239

Gurnett, D. A., & Frank, L. A. (1973). Observed relationships between electric fields and auroral particle precipitation, *J. Geophys. Res., 78,* 145, 1973.

Gurnett, D. A., & Goertz, C. K. (1981). Multiple Alfvén wave reflections excited by Io: Origin of the Jovian decametric arcs. Journal of Geophysical Research, 86(A2), 717–722. https://doi.org/10.1029/JA086iA02p00717

Hebden, S. R., T. R. Robinson, D. M. Wright, T. Yeoman, T. Raita, and T. Bösinger (2005), A quantitative analysis of the diurnal evolution of ionospheric Alfvén resonator magnetic resonance features and calculation of changing IAR parameters, *Ann. Geophys., 23,* 1711.

Hinson, D. P., Flasar, F. M., Kliore, A. J., Schinder, P. J., Twicken, J. D., & Herrera, R. G. (1997). Jupiter's ionosphere: Results frm the first Galileo radio occultation experiment, *Geophysical Research Letters, 24,* 2107-2110.

Hinson, D. P., Twicken, J. D., & Tuna Karayel, E. (1998). Jupiter's ionosphere: New results from Voyager 2 radio occultation measurements, *Journal of Geophysical Research, 103*(A5), 9505-9520.

Hinton, P. C., Bagenal, F., & Bonfond, B. (2019). Alfvén wave propagation in the Io plasma torus. Geophysical Research Letters, 46, 1242–1249. https://doi.org/10.1029/2018GL081472

Hirano, Y., H. Fukunishi, R. Kataoka, T. Hasunuma, T. Nagatsuma, W. Miyake, and A. Matsuoka (2005), Evidence for the resonator of inertial Alfvén waves in the cusp topside ionosphere, *J. Geophys. Res., 110,* A07218, doi: 10.1029/2003JA010329.

Hodges, A., Steffes, P., Bellotti, A., Waite, J. H., Brown, S., Oyafuso, F., et al. (2020). Observations and electron density retrievals of Jupiter's discrete auroral arcs using the Juno Microwave Radiometer. *Journal of Geophysical Research: Planets, 125,* e2019JE006293. https://doi.org/10.1029/2019JE006293

Karlsson, T. (2012). The acceleration region of stable auroral arcs, in A. Keiling, E. Donovan, F. Bagenal, T. Karlsson (eds.) *Auroral Phenomenology and Magnetospheric Processes: Earth and Other Planets, Geophysical Monograph Series* (vol. 197, pp. 227-240). Washington, DC: American Geophysical Union.

Kurth, W. S., Hospodarsky, G. B., Kirchner, D. L., Mokrzycki, B. T., Averakamp, T. F., Robison, W. T., et al. (2017). The Juno Waves investigation, *Space Sci. Rev., 213,* pp. 347-392, doi: 10.1007/s11214-017-0396-y.

Lynch, K. A., Hampton, D. L., Zettergren, M., Bekkeng, T. A., Conde, M., Fernandes, P. A. et al. (2015), MICA sounding rocket observations of conductivity-gradient-generated auroral ionospheric responses: Small-scale structure with large-scale drivers, *J. Geophys. Res. Space Physics,* 120, 9661–9682, doi:10.1002/2014JA020860.

Lysak, R. L. (1991), Feedback instability of the ionospheric resonant cavity, *J. Geophys. Res., 96,* 1553.

Lysak, R. L. (1993), Generalized model of the ionospheric Alfven resonator, in R. L. Lysak (Ed.) *Auroral Plasma Dynamics,* Geophysical Monograph Series (vol. 80, p. 121). Washington, DC: American Geophysical Union.

Lysak, R. L., & Song, Y. (2008), Propagation of kinetic Alfvén waves in the ionospheric Alfvén resonator in the presence of density cavities, *Geophys. Res. Lett., 35,* L20101, doi:10.1029/2008GL035728.

Lysak, R. L., & Song, Y. (2020). Field line resonances in Jupiter's magnetosphere, *Geophysical Research Letters, 47,* e2020GL089473. https://doi.org/10.1029/2020GL089473

Lysak, R. L., Waters, C. L., & Sciffer, M. D. (2013), Modeling of the ionospheric Alfvén resonator in dipolar geometry, *J. Geophys. Res. Space Physics, 118,* doi: 10.1002/jgra.50090.

Mann, I. R., Wright, A. N., & Cally, P. S. (1995), Coupling of magnetospheric cavity modes to field line resonances: a study of resonant widths, *J. Geophys. Res., 100,* 19,441.

Manners, H. A., Masters, A., & Yates, J. N. (2018). Standing Alfvén waves in Jupiter's magnetosphere as a source of ∼10- to 60-min quasiperiodic pulsations. *Geophysical Research Letters, 45,* 8746–8754, https://doi.org/10.1029/2018GL078891

Manners, H. A., & Masters, A. (2019). First evidence for multiple-harmonic standing Alfvén waves in Jupiter's equatorial plasma sheet. *Geophysical Research Letters, 46,* 9344–9351. https://doi.org/10.1029/2019GL083899

Manners, H. A., & Masters, A. (2020). The global distribution of ultralow-frequency waves in Jupiter's magnetosphere. *Journal of Geophysical Research: Space Physics, 125,* e2020JA028345. https://doi.org/10.1029/2020JA028345

Mauk, B. H., Haggerty, D. K., Paranicas, C., Clark, G., Kollman, P., Rymer, A. M., et al. (2017), Discrete and broadband electron acceleration in Jupiter's powerful aurora, *Nature, 549,* 66, doi: 10.1038/nature23648

McComas, D. J., Alexander, N., Allegrini, F., Bagenal, F., Beebe, C., Clark, G., et al. (2017). *Space Science Reviews, 213,* 547-643. doi: 10.1007/s11214-013-9990-9

Miles, D. M., Mann, I. R., Pakhotin, I. P., Burchill, J. K., Howarth, A. D., Knudsen, D. J., et al. (2018). Alfvénic dynamics and fine structuring of discrete auroral arcs: Swarm and e-POP observations. *Geophysical Research Letters, 45.* https://doi.org/10.1002/2017GL076051

Millward, G., Miller, S., Stallard, T., Aylward, A. D., & Achilleos, N. (2002). On the dynamics of the Jovian ionosphere and thermosphere. III. The modeling of auroral conductivity, *Icarus, 160,* 95-107. https://doi.org/10.1006/icar.2002.6951

Miura, A., & Sato, T. (1980), Numerical simulation of the global formation of auroral arcs, *J. Geophys. Res., 85,* 73.

Moriano, A., Mura, A., Adriani, A., Dold, V., Bonfond, B., Waite, J. H., Hue, V. et al. (2021). Morphology of the auroral tail of Io, Europa and Ganymede from JIRAM L-band imager, *Journal of Geophysical Research: Space Physic.*

Mura, A., Adriani, A., Connerney, J. E. P., Bolton, S., Altieri, F., Bagenal, F., et al. (2018). Juno observations of spot structures and a split tail in Io-induced aurorae on Jupiter, *Science, 361,* 774-777. https://doi.org/10.1126/science.aat1450

Mozer, F. S., Cattell, C. A., Hudson, M. K., Lysak, R. L., Temerin, M. & Torbert, R. B. (1980). Satellite measurements and theories of auroral particle acceleration, *Space Sci. Revs., 27,* 155.

Neubauer, F. M. (1980). Nonlinear standing Alfvén wave current system at Io: Theory, *J. Geophys. Res., 85,* 1171-1178.

Pakhotin, I. P., Mann, I. R., Lysak, R. L., Knudsen, D. J., Gjerloev, J. W., Rae, I. J. et al. (2018). Diagnosing the role of Alfvén waves in magnetosphere ionosphere coupling: Swarm observations of large amplitude nonstationary magnetic perturbations during an interval of northward IMF. *Journal of Geophysical Research: Space Physics, 123.* https://doi.org/10.1002/2017JA024713.

Persoon, A. M., D. A. Gurnett, W. K. Peterson, J. H. Waite, J. L. Burch, and J. L. Green (1988), Electron density depletions in the nightside auroral zone, *J. Geophys. Res., 93,* 1871.

Polyakov, S. V., and Rapoport, V. O. (1981), Ionospheric Alfvén resonator, *Geomag. Aeronomy, 21,* 816.

Ray, L. C., Su, Y.-J., Ergun, R. E., Delamere, P. A. & Bagenal, F. (2009), Current-voltage relation of a centrifugally confined plasma, *J. Geophys. Res., 114,* A04214, doi:10.1029/2008JA013969.

Saur, J., Pouquet, A., & Matthaeus, W. H. (2003), An acceleration mechanism for the generation of the main auroral oval on Jupiter, *Geophys. Res. Lett., 30,* 1260, doi: 10.1029/2002GL015761.

Saur, J., Janser, S., Schreiner, A., Clark, G., Mauk, B. H., Kollman, P., et al. (2018), Wave-particle interaction of Alfvén waves in Jupiter's magnetosphere: Auroral and magnetospheric particle acceleration. *Journal of Geophysical Research: Space Physics,* 123, 9560–9573, https://doi.org/10.1029/2018JA025948

Semeter, J., & Blixt, E. M. (2006). Evidence for Alfvén wave dispersion identified in high-resolution auroral imagery, *Geophys. Res. Lett., 33,* L13106, doi:10.1029/2006GL026274.

Singer, H. J.., Southwood, D. J., Walker, R. J., & Kivelson, M. G. (1981), Alfvén wave resonances in a realistic magnetospheric magnetic field geometry, *J. Geophys. Res., 86,* 4589.

Song, Y., & Lysak, R. L. (2006), The displacement current and the generation of parallel electric fields, *Phys. Rev. Lett*., *96,* 145002.

Su, Y., Jones, S. T., Ergun, R. E., Bagenal, F., Parker, S. E., Delamere, P. A., & Lysak, R. L. (2006), Io-Jupiter interaction: Alfvén wave propagation and ionospheric Alfvén resonator, *J. Geophys. Res., 111,* A06211, doi:10.1029/2005JA011252.

Sulaiman, A. H., Hospodarsky, G. B., Elliott, S. S., Kurth, W. S., Gurnett, D. A., Imai, M., et al. (2020). Wave-particle interactions associated with Io's auroral footprint: Evidence of Alfvén, ion cyclotron, and whistler modes. *Geophysical Research Letters, 47,* e2020GL088432. https://doi.org/10.1029/2020GL088432

Sydorenko, D., Rankin, R., and Kabin, K. (2008), Nonlinear effects in the ionospheric Alfvén resonator, *J. Geophys. Res., 113,* A10206, doi:10.1029/2008JA013579.

Szalay, J. R., Allegrini, F., Bagenal, F., Bolton, S. J., Clark, G., Connerney, J. E. P., et al. (2021). Proton outflow associated with Jupiter's auroral processes. *Geophysical Research Letters, 48,* e2020GL091627. https://doi.org/10.1029/2020GL091627

Szalay, J. R., Bonfond, B., Allegrini, F., Bagenal, F., Bolton, S., Clark, G.. et al. (2018), In situ observations connected to the Io footprint tail aurora, *J. Geophys. Res.: Planets, 123,* 3061, doi: https://doi.org/10.1029/2018JE005752

Trakhtengertz, V. Y., and Feldstein, A. Y. (1984), Quiet auroral arcs: ionospheric effect of magnetospheric convection stratification, Planet. Space Sci., 32, 127.

Watt, C. E. J., and Rankin, R. (2009), Electron trapping in shear Alfvén waves that power the aurora, *Phys. Rev. Lett., 102*(4), 045002.

Weiss, J. W. (2004). Planetary parameters, in F. Bagenal, T. E. Dowling, W. B. McKinnon (Eds.) *Jupiter: The Planet, Satellites and Magnetosphere.* Cambridge, UK: Cambridge University Press.

Woodroffe, J. R., & Lysak, R. L. (2012), Ultra-low frequency wave coupling in the ionospheric Alfvén resonator: Characteristics and implications for the interpretation of ground magnetic fields, *J. Geophys. Res.*, 117, A03223, doi:10.1029/2011JA017057.

Yates, J. N., Achilleos, N., & Guio, P. (2014), Response of the Jovian thermosphere to a transient pulse in solar wind pressure, *Planet. Space Sci., 91*, 27.

Yates, J. N., Ray, L. C., Achilleos, N., Witasse, O. G., & Altobelli, N. (2020). Magnetosphere-ionosphere-thermosphere coupling at Jupiter using a three-dimensional atmospheric general circulation model. *Journal of Geophysical Research: Space Physics, 125,* e2019JA026792. https://doi.org/10.1029/2019JA026792

Figure Captions

Figure 1. Profiles of the Alfvén speed (solid curve) and density (dashed curve) for the idealized ionospheric Alfvén speed profile of equation (2).

Figure 2. Amplitude of the electric field, normalized to the incident wave amplitude for the IAR profile of Figure 1. Enhancements of the wave field at normalized frequencies of 2.4, 5.5 and 8.6 are evident.

Figure 3. Plot of the simulation volume, with some representative field lines plotted along with the curves at constant scalar potential that gives the coordinate parallel to the magnetic field.

Figure 4. Alfvén speed (solid) and density (dashed) profiles for the runs shown

Figure 5. Plot of the log of the Alfvén speed overlaid on the grid of Figure 3. Inset: blowup of ionospheric Alfvén resonator region.

Figure 6. Profiles of the (a) electric field and (b) magnetic field for a run in which a 0.25 second pulse was input from the ionospheric end of the simulation region.

Figure 7. Fourier transform of the electric field of Figure 5a, showing resonant frequencies at 0.8 and 1.8 Hz.

Figure 8. Response of the magnetic field to a driver at the (a) resonant frequency of 0.8 Hz; and (b) at a non-resonant frequency of 0.4 Hz. The response is about 5 times greater at the resonant frequency.

Figure 9. Time history of the magnetic field at 17° co-latitude for a run including the parallel electric field. The modulation of the field is due to the reflections from the boundary of the plasma sheet.

Figure 10. Integrated parallel electric field for the run of Figure 8. Reflections from the plasma sheet lead to the enhancement of the parallel potential drop on a 15-second time scale.

Figure 11. Contours of Poynting flux mapped to ionospheric heights at times of (a) 10 seconds; (b) 40 seconds; (c) 80 seconds; and (d) 120 seconds into the run. Green/red colors indicate upward Poynting flux and blue downward. After 10 seconds, the wave is moving upward from the ionosphere. By 40 seconds wave has reflected from the Alfvén speed gradient at about 10 R_J

and is returning to the ionosphere. At later times, the Poynting flux is alternative in sign, indicative of a standing wave. As the run progresses, there is increased structure in the perpendicular direction due to phase mixing.

Figure 12. Maximum potential for a run in which the ionospheric scale height is decreased to 4100 km, leading to a density of about 1 cm^{-3} at 1.7 R_J.

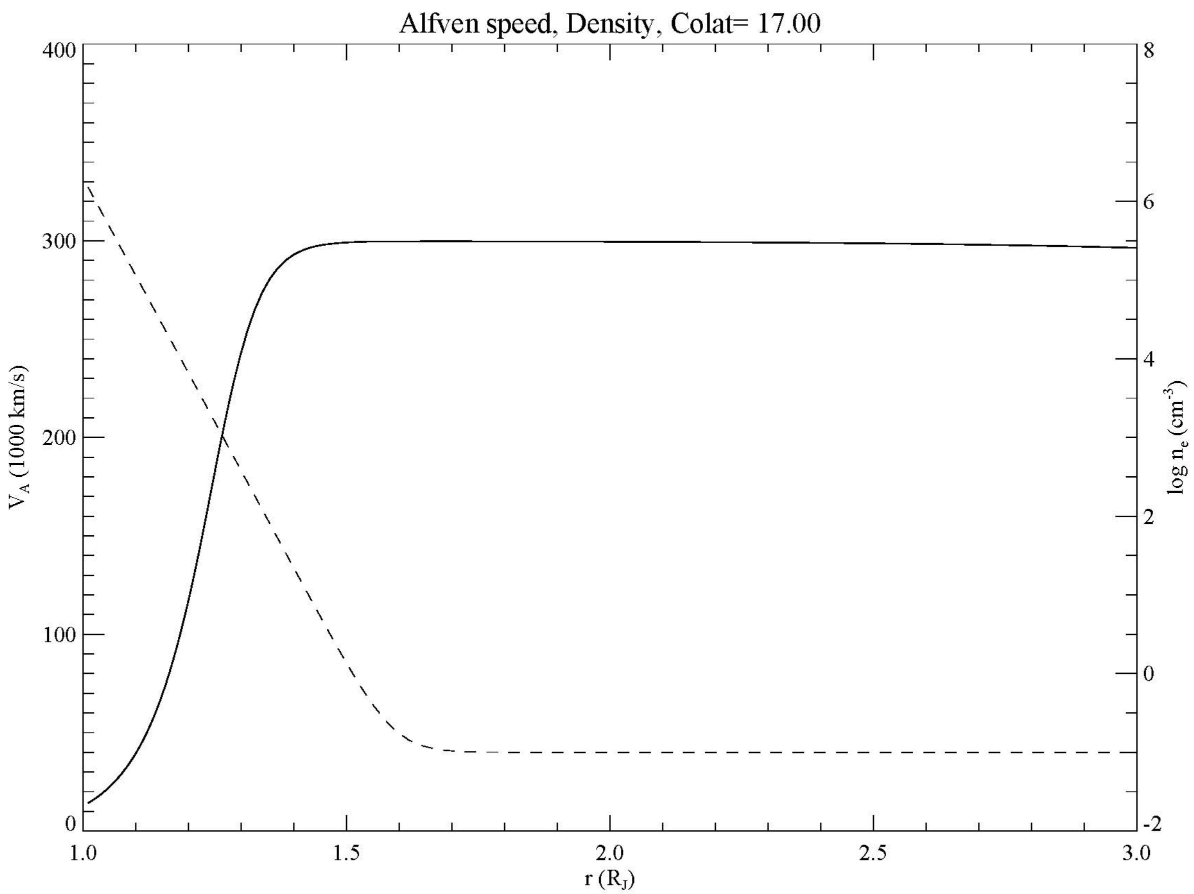

Figure 1. Profiles of the Alfvén speed (solid curve) and density (dashed curve) for the idealized ionospheric Alfvén speed profile of equation (2).

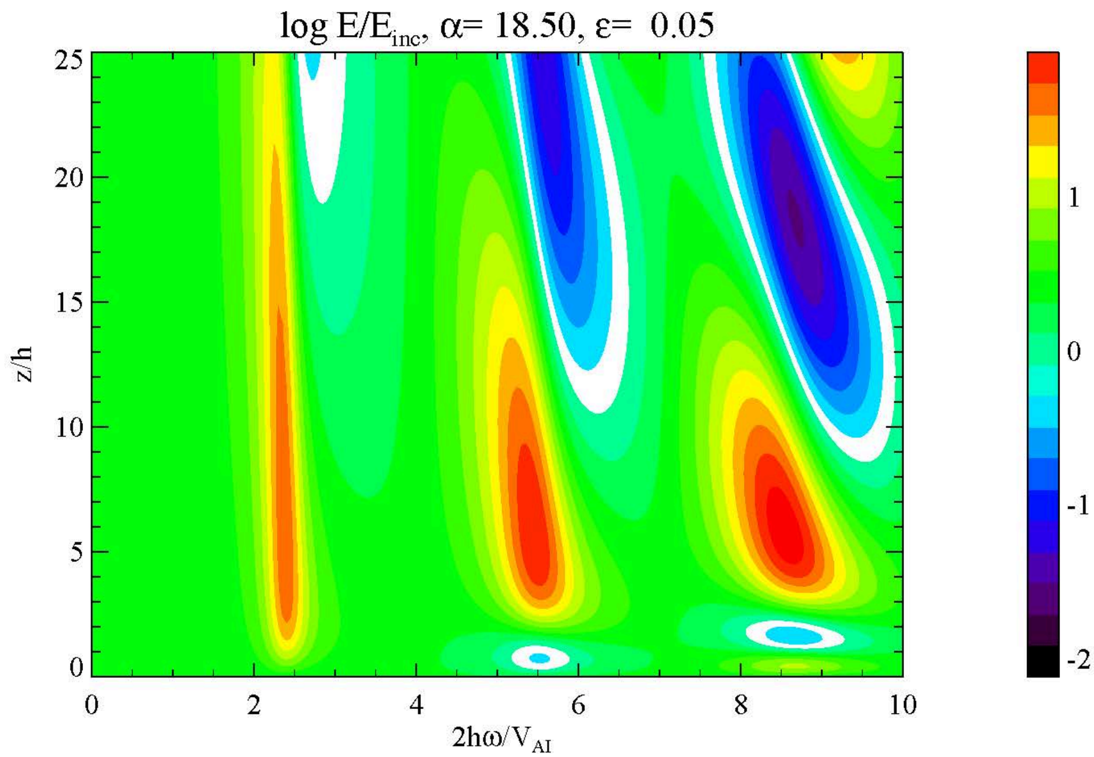

Figure 2. Amplitude of the electric field, normalized to the incident wave amplitude for the IAR profile of Figure 1. Enhancements of the wave field at normalized frequencies of 2.4, 5.5 and 8.6 are evident.

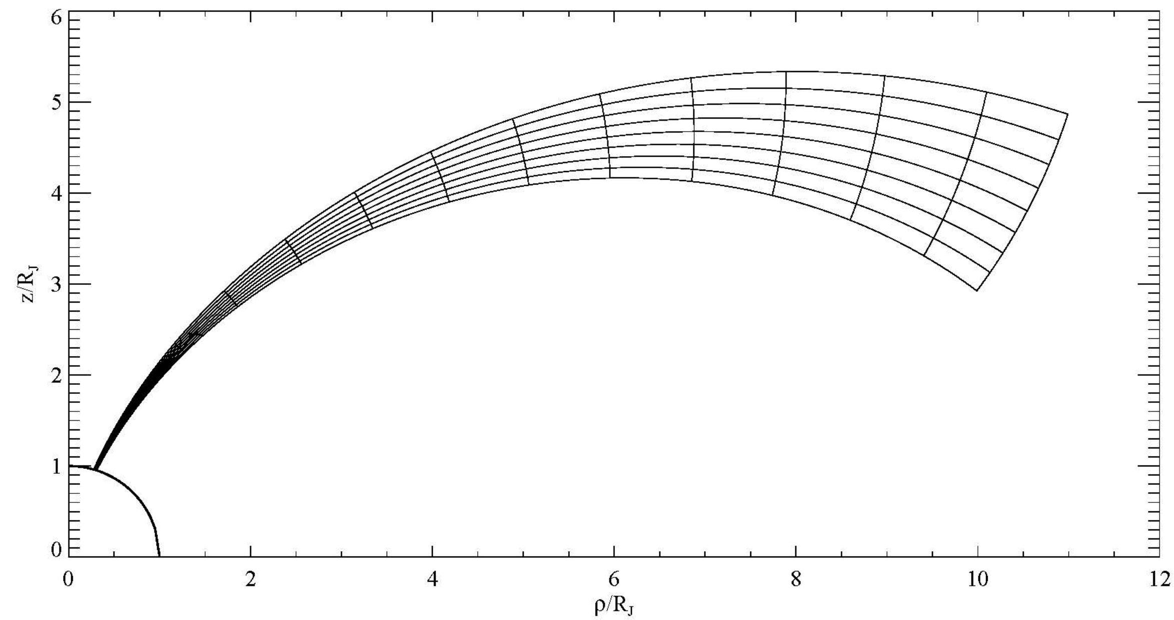

Figure 3. Plot of the simulation volume, with some representative field lines plotted along with the curves at constant scalar potential that gives the coordinate parallel to the magnetic field. The bracket indicates the region of the ionospheric Alfvén resonator where the main acceleration will take place.

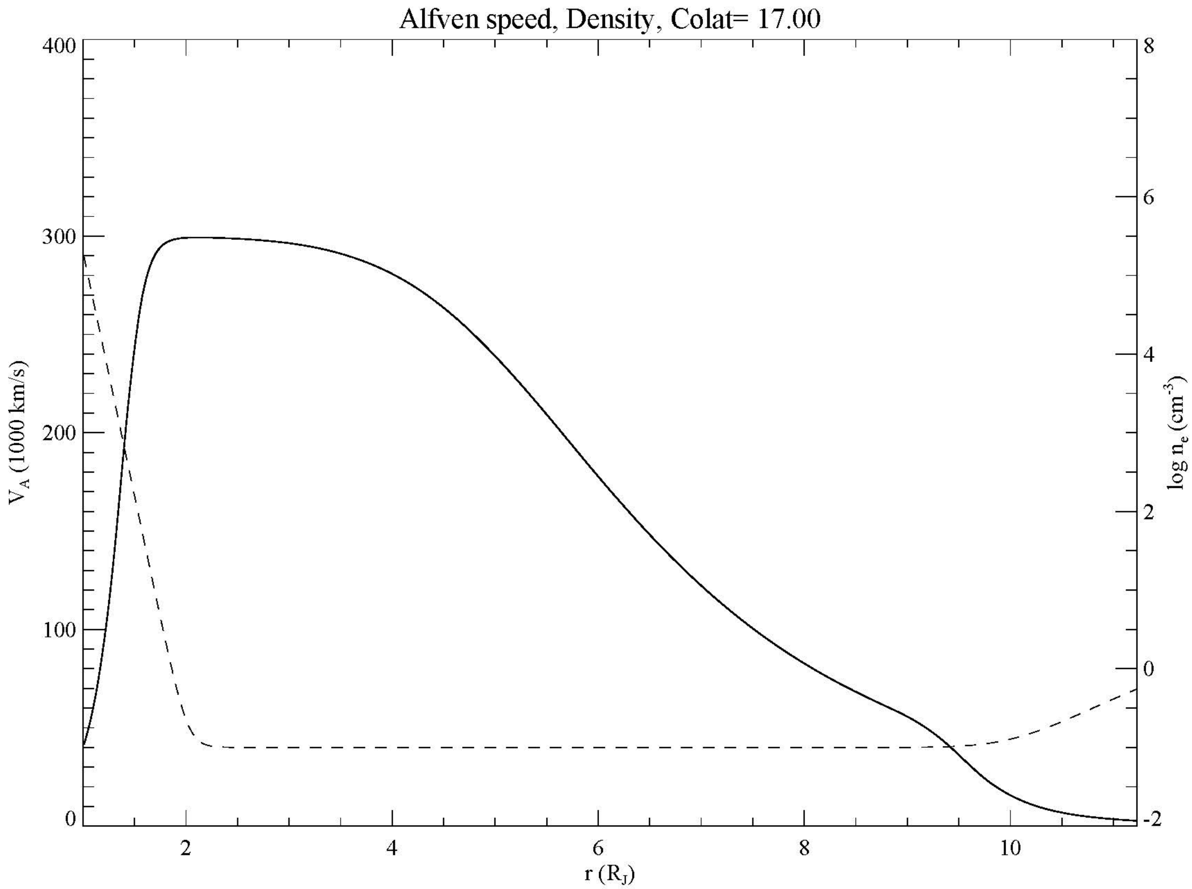

Figure 4. Profiles of the Alfvén speed (solid) and density (dashed) for the runs shown

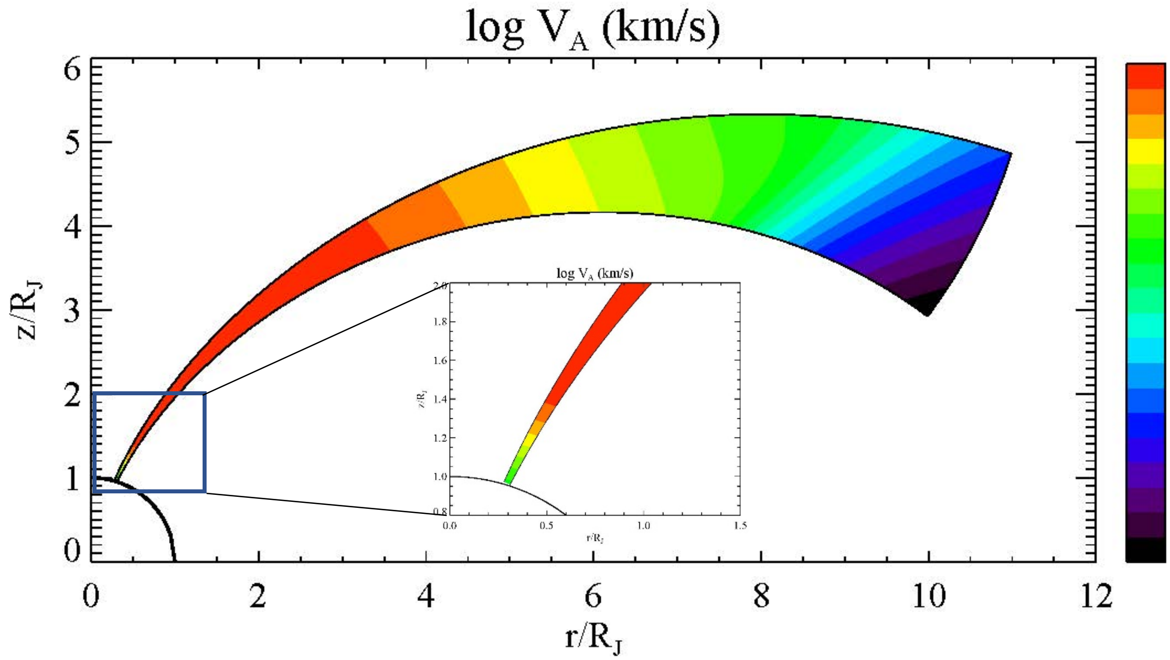

Figure 5. Plot of the log of the Alfvén speed overlaid on the grid of Figure 3. Inset: blowup of ionospheric Alfvén resonator region.

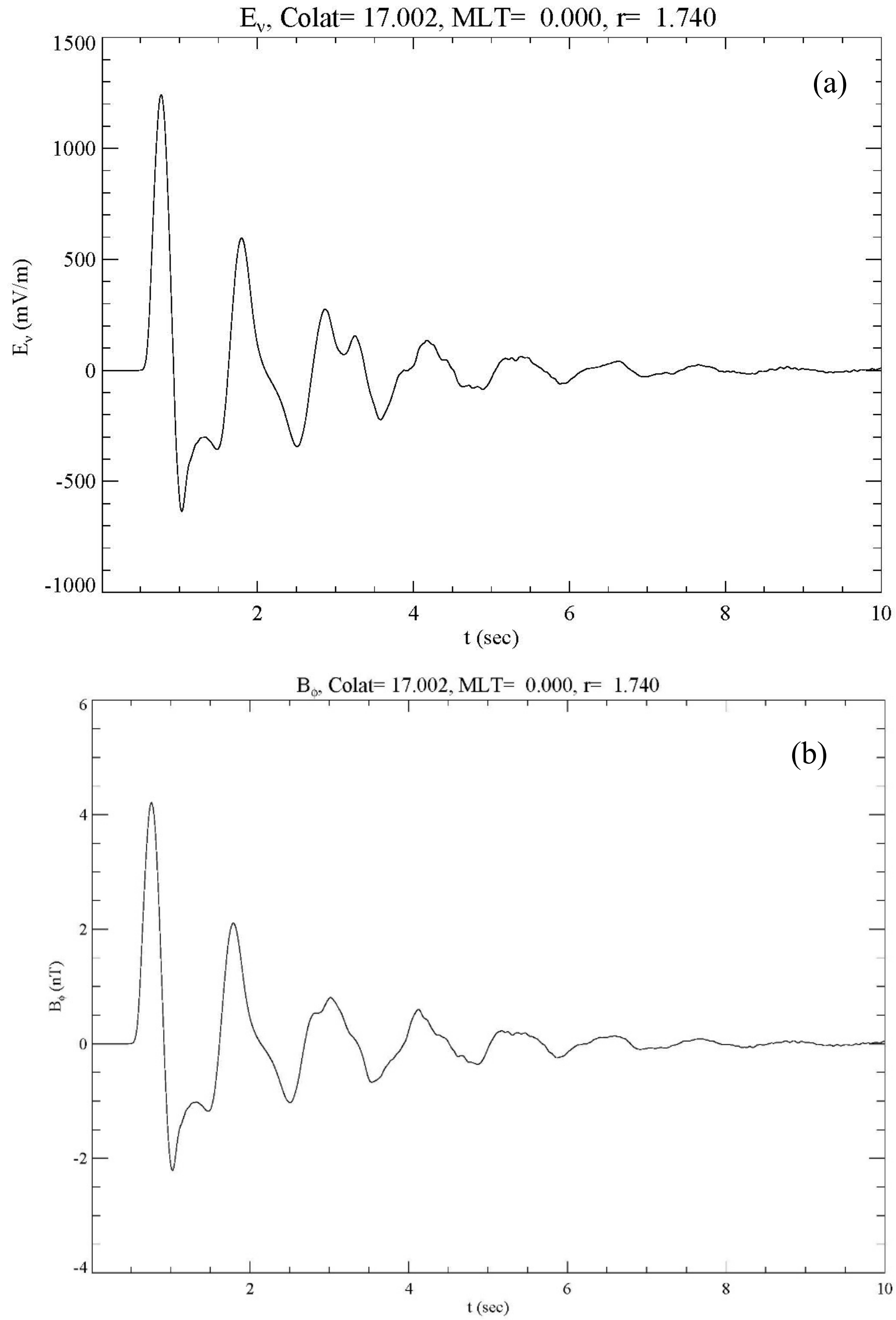

Figure 6. Profiles of the (a) electric field and (b) magnetic field for a run in which a 0.25 second pulse was input from the ionospheric end of the simulation region.

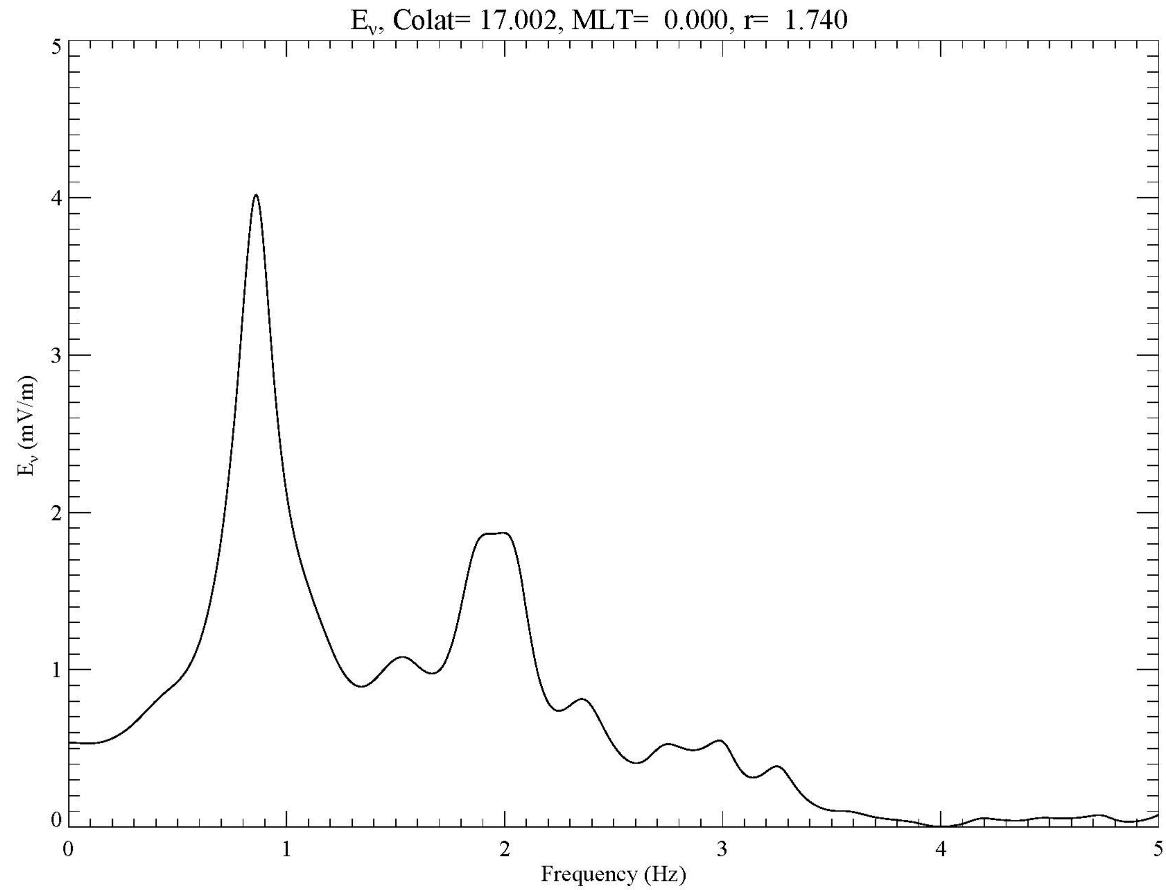

Figure 7. Fourier transform of the electric field of Figure 5a, showing resonant frequencies at 0.8 and 1.8 Hz.

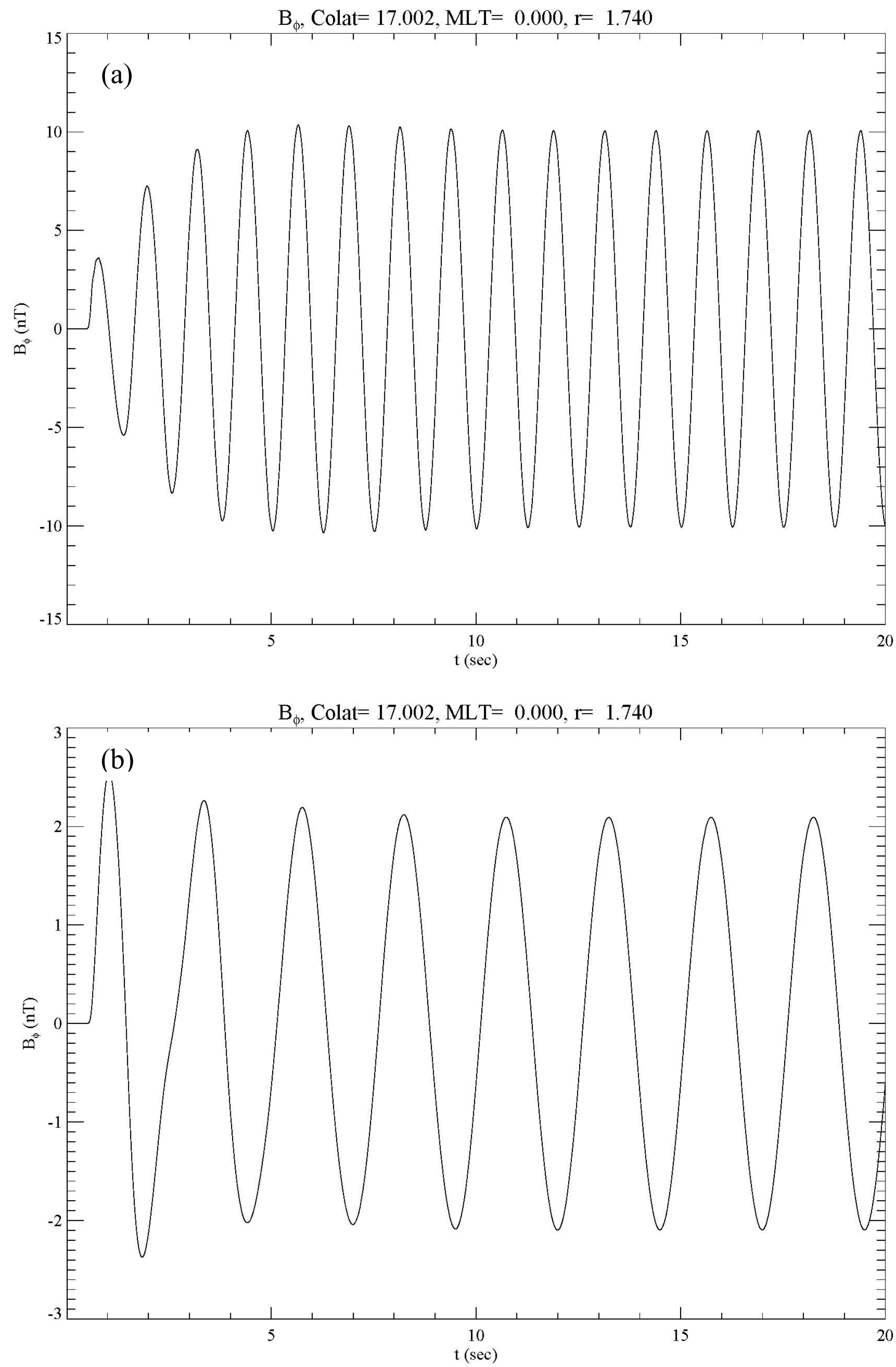

Figure 8. Response of the magnetic field to a driver at the (a) resonant frequency of 0.8 Hz; and (b) at a non-resonant frequency of 0.4 Hz. The response is about 5 times greater at the resonant frequency.

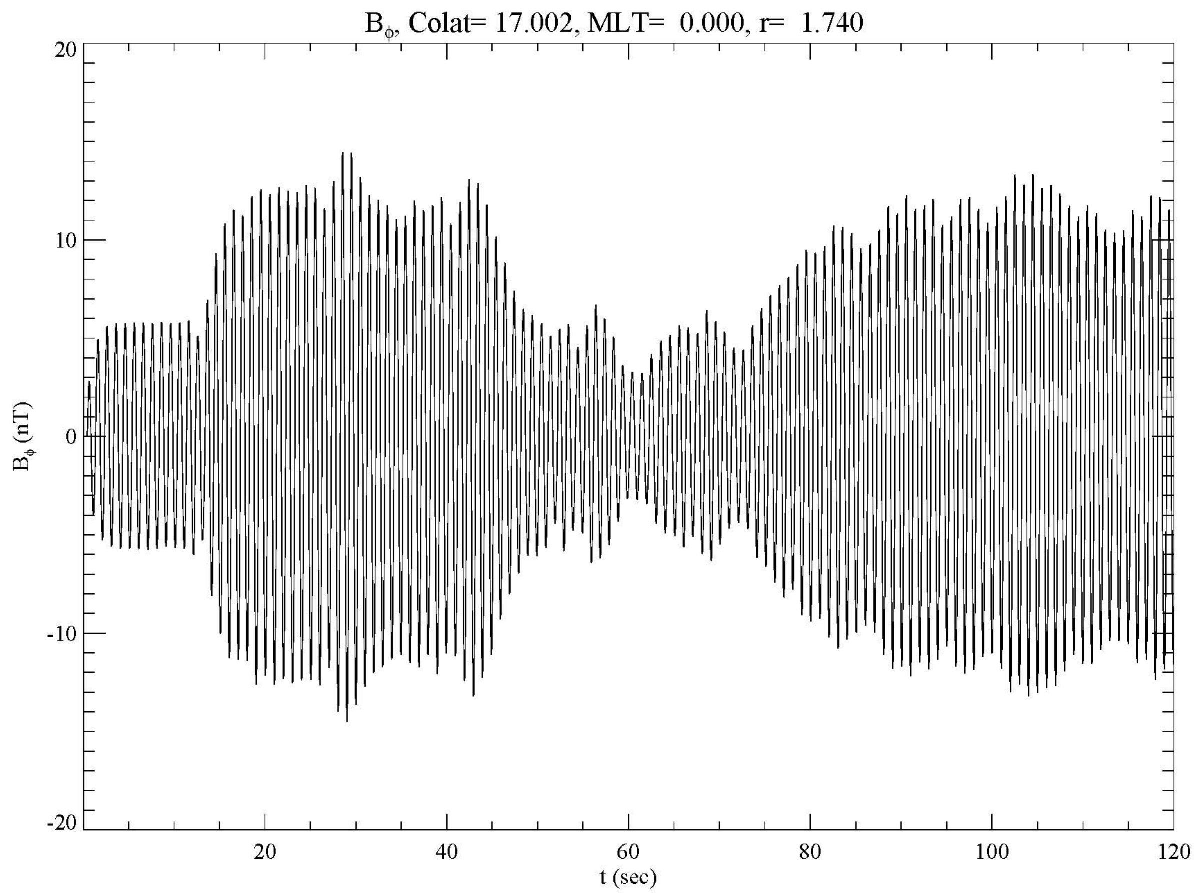

Figure 9. Time history of the magnetic field at 17° co-latitude for a run including the parallel electric field. The modulation of the field is due to the reflections from the boundary of the plasma sheet.

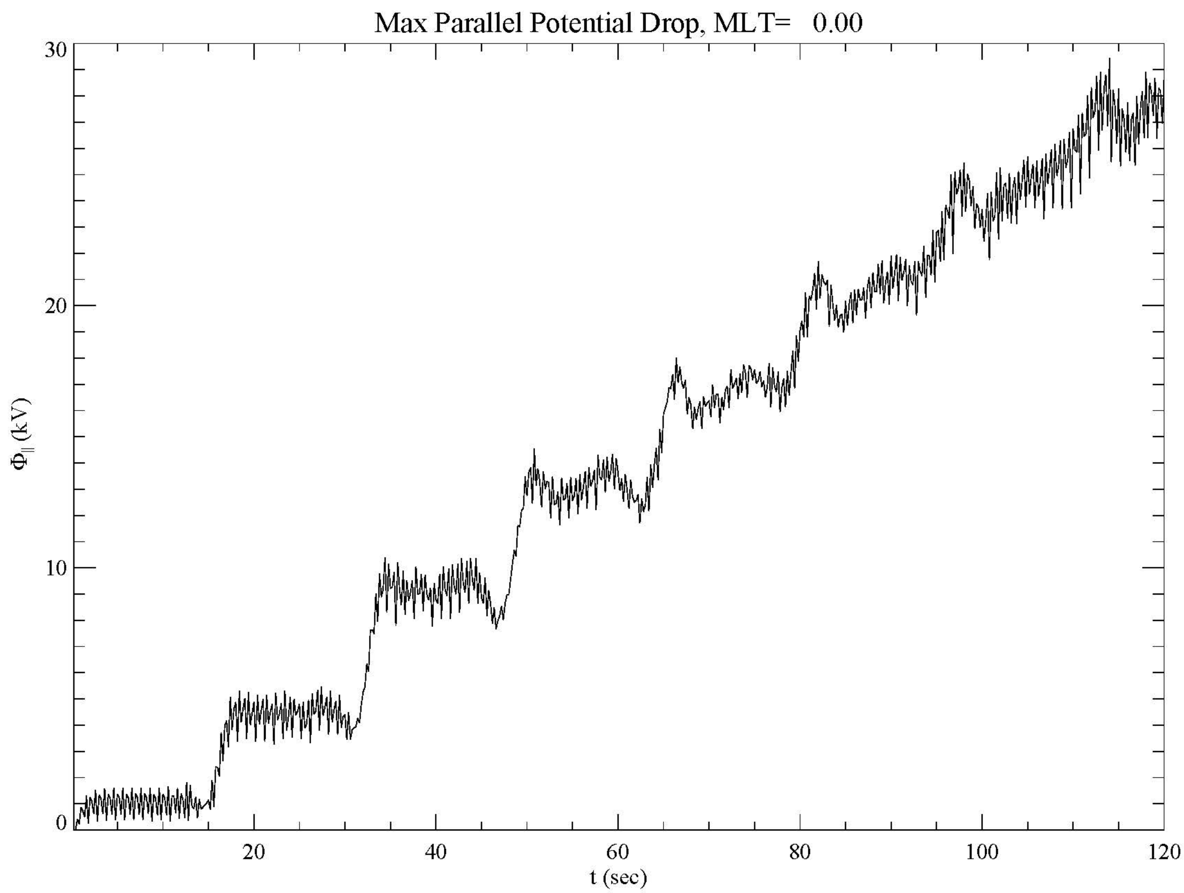

Figure 10. Integrated parallel electric field for the run of Figure 8. Reflections from the plasma sheet lead to the enhancement of the parallel potential drop on a 15-second time scale.

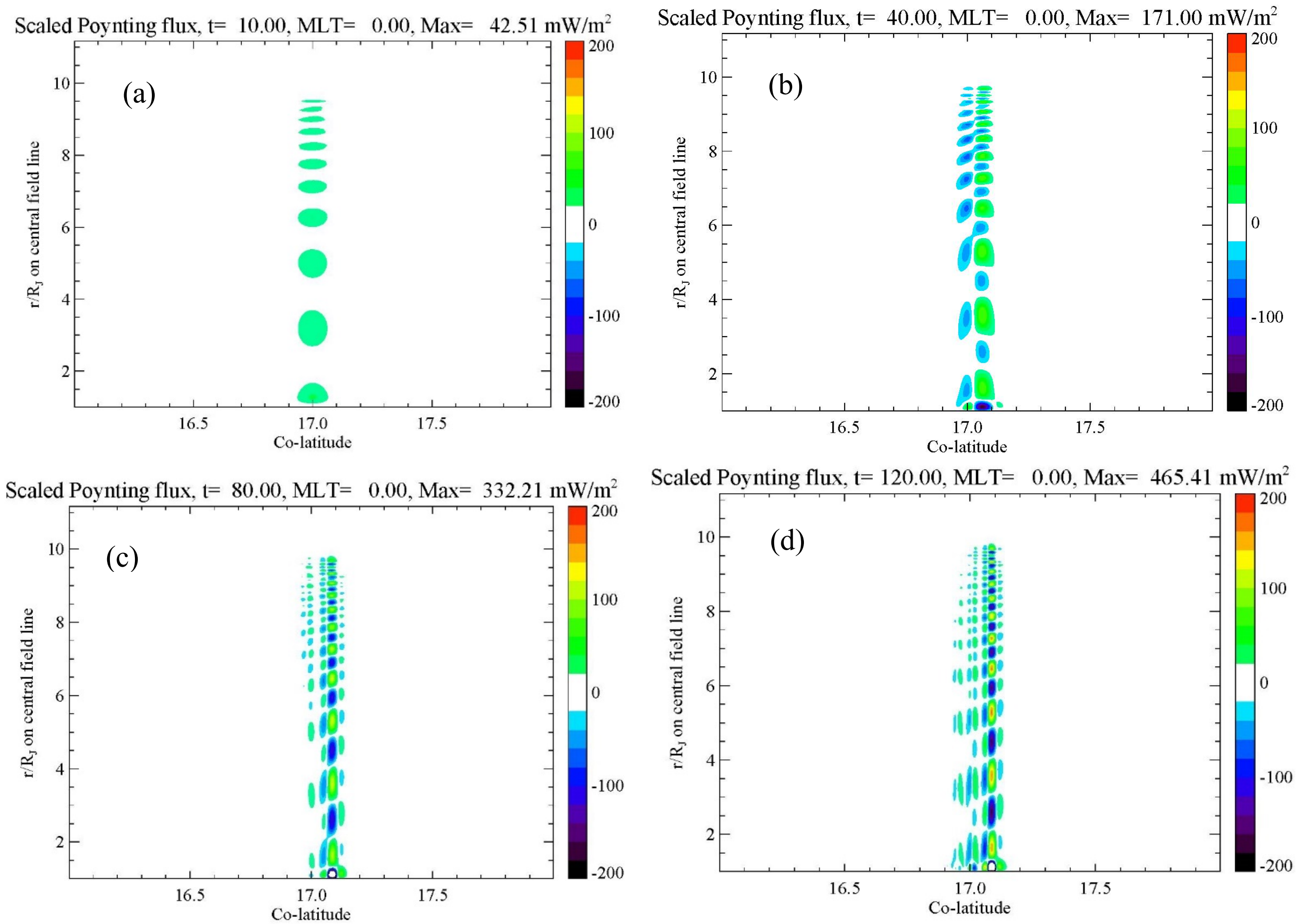

Figure 11. Contours of Poynting flux mapped to ionospheric heights at times of (a) 10 seconds; (b) 40 seconds; (c) 80 seconds; and (d) 120 seconds into the run. Green/red colors indicate upward Poynting flux and blue downward. After 10 seconds, the wave is moving upward from the ionosphere. By 40 seconds wave has reflected from the Alfvén speed gradient at about 10 R_J and is returning to the ionosphere. At later times, the Poynting flux is alternative in sign, indicative of a standing wave. As the run progresses, there is increased structure in the perpendicular direction due to phase mixing.

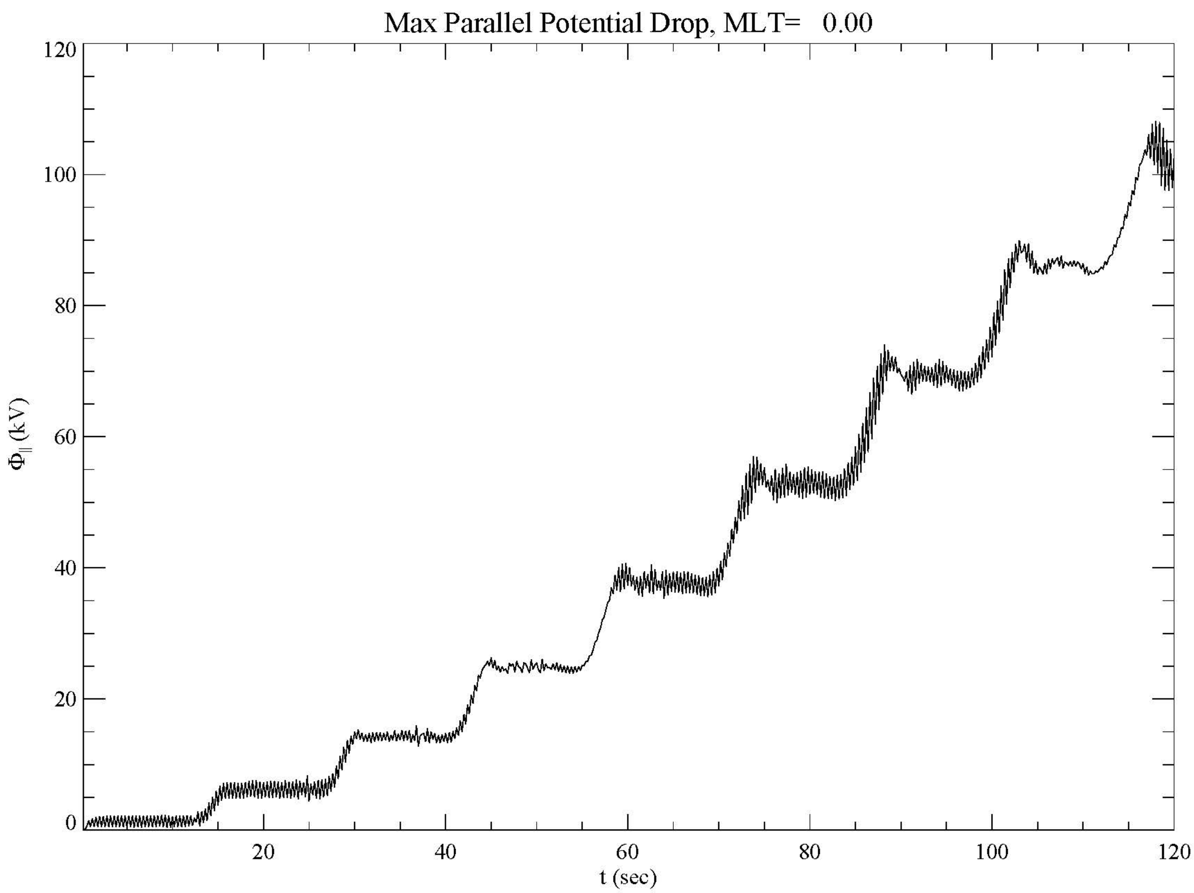

Figure 12. Maximum potential for a run in which the ionospheric scale height is decreased to 4100 km, leading to a density of about 1 cm^{-3} at 1.7 R_J.